



available at www.sciencedirect.com



journal homepage: www.elsevier.com/locate/jhydrol



Numerical simulation of the effect of the sloping submarine outlet-capping on tidal groundwater head fluctuation in confined coastal aquifers

Shuang Liu ^{a,b}, Hailong Li ^{a,b,c,*}, Michel C. Boufadel ^c, Guohui Li ^a

^a School of Environmental Studies and (MOE) Biogeology and Environmental Geology Laboratory, China University of Geosciences, Wuhan 430074, PR China

^b Department of Mathematics, Anshan Normal University, Anshan 114005, PR China

^c Department of Civil and Environmental Engineering, Temple University, 1947 North 12th Street, Philadelphia, PA 19122, United States

Received 30 November 2007; received in revised form 3 August 2008; accepted 7 August 2008

KEYWORDS

Numerical simulation;
Sloping submarine outlet-capping;
Loading efficiency;
Coastal confined aquifer;
Tide-induced head fluctuation

Summary The submarine outlet of a coastal confined aquifer is usually covered by less-permeable material such as silt and fine sand which forms a sloping or almost flat seabed. Previous analytical studies of the tide-induced head fluctuation usually assumed a vertical interface between the outlet-capping and the seawater and neglected the effects of the outlet-capping's slope. Here we conducted a series of numerical simulations to investigate the effect of the slope of the outlet-capping on the tide-induced head fluctuations in a coastal confined aquifer. The numerical simulations demonstrated that when the hydraulic diffusivity, slope and/or the outlet-capping leakance are large, the tidal loading effect is relatively weak and the leakance dominates. In this case the analytical solution applies. In general, the joint actions of the outlet-capping leakance and the tidal loading effects result in complicated, 2-dimensional flow in the aquifer near the shoreline. For aquifers with small hydraulic diffusivity, small slope and/or small outlet-capping leakance, the outlet acts approximately as a no-flow boundary condition and the tidal loading dominates. In this case, negative phase shifts (time-advance) may occur near the coastline. The study provides potential guide to infer the aquifer's submarine structure and parameter from tidal head fluctuation observations in inland wells.

Published by Elsevier B.V.

* Corresponding author. Address: Department of Civil and Environmental Engineering, Temple University, 1947 N. 12th Street, Philadelphia, PA 19122, United States. Tel.: +1 215 204 8428; fax: +1 215 204 4696.

E-mail addresses: liushuang78@gmail.com (S. Liu), hailong@graduate.hku.hk (H. Li), boufadel@temple.edu (M.C. Boufadel), whguohui@gmail.com (G. Li).

Introduction

Since the 1950s, many analytical solutions have been derived to investigate the tide-induced periodic groundwater flow in confined coastal aquifers (e.g., Jacob, 1950; van der Kamp, 1972; Li and Chen, 1991a,b; Jeng et al., 2002; Li et al., 2000a; Townley, 1995; Sun, 1997; Jiao and Tang, 1999; Li and Jiao, 2001a,b; Li et al., 2002). In these studies, the seaward boundary (the aquifer's submarine outlet) was assumed to be hydraulically directly connected to the sea. In reality, the submarine outlet of a coastal aquifer is usually covered by a less-permeable material such as silt and fine sand (Li and Chen, 1991b; Li et al., 2007; Xia et al., 2007). The effects of this submarine outlet-capping have been studied recently analytically by Li et al. (2007), Xia et al. (2007) and Guo et al. (2007) with an assumption that the interface between the outlet-capping and the seawater is vertical. Li et al. (2007) considered the effect of the offshore extent of a single confined submarine aquifer. When the offshore extent is zero (i.e., the outlet-capping is vertical and located at the coastline), they found that the head in the confined aquifer is given by

$$h(x, t) = \frac{A\sigma e^{-ax} \cos(\omega t - ax - \arctan \frac{1}{1+\sigma})}{\sqrt{\sigma^2 + 2\sigma + 2}}, \quad x \geq 0, \quad (1a)$$

where A is the amplitude of tide [L], $\omega = 2\pi/t_0$ is the tidal angular velocity [T^{-1}], and t_0 is the tidal period [T]. The parameters a and σ are termed as the confined aquifer's tidal propagation parameter [L^{-1}] and the dimensionless leakage of the outlet-capping, respectively. They are defined as follows:

$$a = \sqrt{\frac{\omega S_s}{2K}}; \quad \sigma = \frac{K'}{amK}, \quad (1b)$$

where S_s and K are the specific storage [L^{-1}] and hydraulic conductivity [LT^{-1}] of the aquifer, respectively; K' and m are the hydraulic conductivity [LT^{-1}] and the horizontal thickness [L] of the outlet-capping, respectively. Eq. (1a) describes the tidal head fluctuation influenced by the vertical outlet-capping with a dimensionless leakage of σ . In the case that there is no outlet-capping, namely, the thickness m tends to zero, the parameter σ tends to infinity and

the solution (1a) becomes the well-known Jacob (1950) solution.

In reality, however, the sea–land boundary (the submarine outlet of the aquifer or its outlet-capping) is usually sloping. In the case the aquifer is unconfined, the effect of the slope beach on the tidal groundwater flow has been investigated by many researchers (e.g., Nielsen, 1990; Li et al., 2000b; Cartwright et al., 2004). In the case that the aquifer is confined, to the best knowledge of the authors, there is no work in literature which addressed the effect of a sloping submarine outlet-capping on the tidal groundwater flow. An attempt was made in this paper to fill this gap. A series of numerical simulations was conducted for various aquifer parameters including different outlet-capping's slopes ranging from 5° to 90° . The numerical results were analysed and compared with the analytical solution which assumes a vertical outlet-capping.

Mathematical model

Mathematical model for tidal groundwater flow

Here we consider a coastal confined aquifer with a sloping submarine outlet-capping as shown in Fig. 1. The model is based on the assumptions that (i) the aquifer is homogeneous and isotropic, (ii) the effects of density variation and the elastic storage of the outlet-capping on the tidal groundwater flow are negligible. For simplicity, here we only consider the case when the offshore extent is zero (i.e., the outlet-capping starts from the coastline), which is commonplace in reality (Xia et al., 2007). Let the x -axis be perpendicular to the coastline and positive landward, with the origin at the coastline, and the z -axis be positive upward (Fig. 1). On the basis of the above assumptions, the tide-induced groundwater flow in the confined aquifer can be described by the following governing equations (van der Kamp, 1972):

In the inland aquifer,

$$S_s \frac{\partial H}{\partial t} = K \left(\frac{\partial^2 H}{\partial x^2} + \frac{\partial^2 H}{\partial z^2} \right), \quad -\infty < t < \infty, \quad 0 < x < \infty, \quad 0 \leq z \leq b; \quad (2)$$

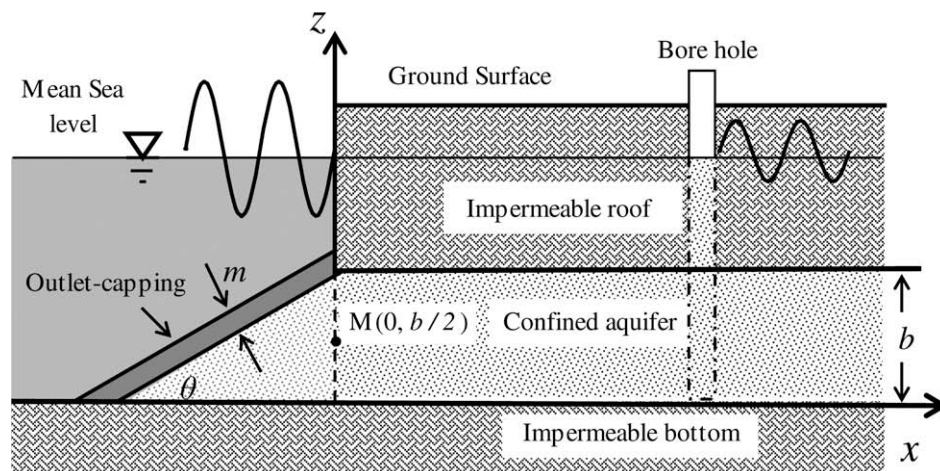


Figure 1 Cross section of a confined aquifer extending under the sea covered by a sloping outlet-capping.

in the offshore part,

$$S_s \frac{\partial H}{\partial t} = K \left(\frac{\partial^2 H}{\partial x^2} + \frac{\partial^2 H}{\partial z^2} \right) + L_e S_s \frac{dh_{sea}}{dt}, \quad -\infty < t < \infty, \quad -bcot \theta \leq x < 0, \quad 0 \leq z \leq x \tan \theta + b, \quad (3)$$

where (x, z) are spatial coordinates and t is time. $H(x, z, t)$ is the hydraulic head [L] of the aquifer; θ is the slope of the outlet-capping; b is the thickness [L] of the confined aquifer; $h_{sea}(t)$ is the sea level [L] given as

$$h_{sea}(t) = A \cos(\omega t), \quad (4)$$

and L_e is the loading efficiency (dimensionless) of the sea tide. The loading efficiency was defined as (Jacob, 1950)

$$L_e = \frac{\alpha}{\alpha + n\beta}, \quad (5)$$

where α is the vertical compressibility [$M^{-1}LT^2$] of the aquifer skeleton, β is the compressibility [$M^{-1}LT^2$] of pore water in the confined aquifer, and n is the porosity (dimensionless) of the aquifer. The loading efficiency defined by Eq. (5) was termed ‘‘amplitude factor’’ by Jacob (1950) and Ferris (1951). Following Jacob (1940), another term ‘‘tidal efficiency’’ was also used for the quantity given by Eq. (5) by many successors such as Carr (1971), Li and Chen (1991a,b) and Li and Jiao (2001a).

It is assumed that there is no inland recharge, so no-flow boundary condition is used at places sufficiently far from the coastline, i.e.,

$$\lim_{x \rightarrow -\infty} \frac{\partial H}{\partial x} = \lim_{x \rightarrow -\infty} \frac{\partial H}{\partial z} = 0, \quad -\infty < t < \infty, \quad 0 < z < b. \quad (6)$$

Because the top and bottom boundaries are impermeable, no-flow boundary conditions are used, i.e.,

$$\left. \frac{\partial H}{\partial z} \right|_{z=b} = 0, \quad -\infty < t < \infty, \quad 0 < x < \infty, \quad (7)$$

$$\left. \frac{\partial H}{\partial z} \right|_{z=0} = 0, \quad -\infty < t < \infty, \quad -bcot \theta < x < \infty. \quad (8)$$

At the coastline $x = 0$, using the continuities of hydraulic head and flux, respectively, yields

$$\lim_{x \rightarrow 0^+} H(x, z, t) = \lim_{x \rightarrow 0^-} H(x, z, t), \quad -\infty < t < \infty, \quad 0 < z < b, \quad (9)$$

$$\lim_{x \rightarrow 0^+} \frac{\partial H}{\partial x} = \lim_{x \rightarrow 0^-} \frac{\partial H}{\partial x}, \quad -\infty < t < \infty, \quad 0 < z < b, \quad (10)$$

$$\lim_{x \rightarrow 0^+} \frac{\partial H}{\partial z} = \lim_{x \rightarrow 0^-} \frac{\partial H}{\partial z}, \quad -\infty < t < \infty, \quad 0 < z < b. \quad (11)$$

Neglecting the elastic storage in the outlet-capping, the flux between the outlet-capping and the aquifer is equal to that between the sea and the outlet-capping. So on the interface Γ between the outlet-capping and the aquifer, using Darcy’s law, one has

$$K \left. \frac{\partial H}{\partial n} \right|_{\Gamma} = K' \frac{h_{sea} - H|_{\Gamma}}{m}, \quad -\infty < t < \infty, \quad -bcot \theta \leq x \leq 0, \quad z = x \tan \theta + b, \quad (12)$$

where n denotes the unit outward normal vector of the interface Γ .

Equivalent time-independent model

The mathematical model Eqs. (2)–(4) and (6)–(12) has nine parameters: A , S_s , K , b , K' , L_e , θ , m and ω . In order to find the minimum number of the independent model parameters, the following complex transformation is introduced

$$H(x, z, t) = A \operatorname{Re}[W(x, z) \exp(i\omega t)], \quad (13)$$

where $i = \sqrt{-1}$, ‘‘Re’’ denotes the real part of the followed complex expression, the dimensionless complex amplitude $W(x, z)$ is a complex function of x and z , its magnitude represents the relative amplitude (ratio of the local fluctuation amplitude to the tidal amplitude A), and its argument, the phase shift (Li et al., 2006). Substituting Eq. (13) into model Eqs. (2)–(4) and (6)–(12), and using the equality

$$h_{sea}(t) = A \cos(\omega t) = \operatorname{Re}[A \exp(i\omega t)], \quad (14)$$

the model Eqs. (2)–(4) and (6)–(12) can be changed into an equivalent time-independent model as follows:

$$\frac{\partial^2 W}{\partial x^2} + \frac{\partial^2 W}{\partial z^2} - i2a^2 W = 0, \quad 0 < x < \infty, \quad 0 \leq z \leq b, \quad (15a)$$

$$\frac{\partial^2 W}{\partial x^2} + \frac{\partial^2 W}{\partial z^2} - i2a^2(W - L_e) = 0, \quad -bcot \theta \leq x < 0, \quad 0 \leq z \leq x \tan \theta + b, \quad (15b)$$

$$\lim_{x \rightarrow -\infty} \frac{\partial W}{\partial x} = \lim_{x \rightarrow -\infty} \frac{\partial W}{\partial z} = 0, \quad 0 < z < b, \quad (15c)$$

$$\left. \frac{\partial W}{\partial z} \right|_{z=b} = 0, \quad 0 < x < \infty, \quad (15d)$$

$$\left. \frac{\partial W}{\partial z} \right|_{z=0} = 0, \quad -bcot \theta < x < \infty, \quad (15e)$$

$$\lim_{x \rightarrow 0^+} W(x, z) = \lim_{x \rightarrow 0^-} W(x, z), \quad 0 < z < b, \quad (15f)$$

$$\lim_{x \rightarrow 0^+} \frac{\partial W}{\partial x} = \lim_{x \rightarrow 0^-} \frac{\partial W}{\partial x}, \quad 0 < z < b, \quad (15g)$$

$$\lim_{x \rightarrow 0^+} \frac{\partial W}{\partial z} = \lim_{x \rightarrow 0^-} \frac{\partial W}{\partial z}, \quad 0 < z < b, \quad (15h)$$

$$\left(\frac{\partial W}{\partial n} + a\sigma W \right) \Big|_{\Gamma} = a\sigma, \quad -bcot \theta \leq x \leq 0, \quad z = x \tan \theta + b. \quad (15i)$$

The equivalent mathematical model Eqs. (15a)–(15i) has five independent parameters: a , b , σ , L_e and θ . Due to the model linearity, the tidal amplitude is eliminated by introducing the relative amplitude. The tidal frequency ω is included in the parameters a and σ . Therefore, the solution of model Eq. (15) is applicable for any tidal frequency (diurnal or semidiurnal) and amplitude.

Model parameter value range and numerical implementation

It is important to find the typical value ranges of the model parameters a , b , σ , L_e and θ for commonplace coastal

aquifer systems. Table 1 of Li and Jiao (2001b) summarized the value ranges of hydrogeological parameters of case studies in coastal aquifers reported in literatures. The parameter a ranges from $9 \times 10^{-4} \text{ m}^{-1}$ to $9 \times 10^{-3} \text{ m}^{-1}$ and the thickness b from 6.1 m to 28 m. Li et al. (1999) used a value of 30 m as the typical thickness of a coastal aquifer. Field observations (e.g., Gregg, 1966, Fig. 6; Carr and van der Kamp, 1969, Table 2; Erskine, 1991, Figs. 4–6) and theoretical analysis of Merritt (2004) demonstrated that the typical value of L_e ranges from 0.05 to 1. Based on the above information, in our numerical simulations, the following parameter value ranges are used: wave number a : $10^{-3.5}$ – 10^{-2} m^{-1} , the aquifer thickness $b = 30 \text{ m}$, the dimensionless leakance σ : 10^{-2} , 1.0 and 10^2 (for representing small, intermediate and large leakance, respectively), L_e : 0.0, 0.5, 0.9 and 1. Four values 5° , 10° , 40° and 70° will be used for the slope θ .

The infinite landward-extent of the model domain (see Eqs. (15a) and (15c)) was approximated by a sufficiently large distance of 7000 m from the coastline to the inland no-flow boundary. The standard Galerkin finite element procedure (see, e.g., Pinder and Gray, 1977) was used to discretize the governing equations using the linear triangle finite elements, and the semi-numerical simulation method of Li et al. (2006) was adopted to obtain the dimensionless complex amplitude of the time-independent model Eq. (15). The mesh contains 3900 triangle elements with constant vertical increment of 1 m. The horizontal increment ranges from 1 m at the coastline to 942 m, increasing landward in a geometrical manner. In the offshore area, the horizontal increment is different constant for different slope θ , and equals $\cot\theta$ m.

Simulation results

Comparison with the analytical solution (1a)

When the slope θ equals 90° , the boundary condition of the outlet-capping becomes that of Li et al. (2007) with zero offshore extent. In this case, the numerical solution of model (2)–(4) and (6)–(12) should be exactly the same as the analytical solution given by Eq. (1a). We plotted the amplitude and phase shift contour lines predicted by analytical solution (1a) and the numerical solutions of model (15) when $\theta = 90^\circ$, $a = 0.01 \text{ m}^{-1}$, and 0.001 m^{-1} , and $\sigma = 0.001$, 0.01, 0.1, 1.0, 10.0, 100.0, and 1000.0. For all the cases the contours of the numerical and analytical solutions coincide with each other completely, giving certain degree of confidence on the numerical method.

Base simulation results

Our model has two forcing terms: the tidal loading effect on the offshore part of the aquifer and the hydraulic connection with tidal water body through the outlet-capping. The first forcing is described by the term $2a^2 L_e$ in Eq. (15b) and the second, by the term $a\sigma$ in the boundary condition (15i). In this section base simulations with individual forcing term will be conducted to investigate the role of each of them in the model. Given the wave number a , the tidal loading efficiency L_e determines the tidal loading forcing

acting on the whole offshore aquifer in Eq. (15b), and the dimensionless leakance σ determines the leaky boundary condition on the interface of the outlet-capping and the aquifer. When σ is great, the boundary condition Eq. (15i) approximately becomes the Dirichlet boundary condition $W|_I = 1$, indicating perfect hydraulic connection between the seawater and aquifer pore water. When σ is small, it approximately becomes the no-flow Neumann boundary condition $\frac{\partial W}{\partial n}|_I = 0$, indicating no hydraulic connection between the seawater and aquifer pore water.

Let W_{loading} be the solution of Eq. (15) when $\sigma = 0$ and $L_e = 1$, and W_{leakage} be the solution of Eq. (15) when $L_e = 0$, then W_{loading} describes the pure, unit tidal loading effect on tidal head fluctuation without leakage and W_{leakage} describes the pure leakage effect through the outlet-capping without loading. Due to the linearity of the model, using the superposition principle, the complex amplitude W (namely, the solution of model Eq. (15)) for any L_e can be expressed in terms of the base functions W_{loading} and W_{leakage} as

$$W = L_e W_{\text{loading}} + W_{\text{leakage}}. \quad (16)$$

Here it should be noted that, due to the term $a\sigma W$ in the boundary condition Eq. (15i), the solution W_{leakage} is not linear with respect to σ . Based on Eq. (16), the behavior of the W function can be demonstrated clearly by simulations for the base functions W_{loading} and W_{leakage} when the wave number a is fixed at different values. For the sake of succinctness, we only analysed the case when the slope is 10° .

Figs. 2 and 3 reported the spatial variations of the base function W_{loading} in aquifer near the shore for different values of the wave number a . The head fluctuation amplitude induced by the pure, unit loading effect is given by $|W_{\text{loading}}|$, and the phase shift, by $\arg(W_{\text{loading}})$. The following observations can be made from Fig. 2. The fluctuation amplitude in the offshore aquifer increases with the wave number a . This is because the forcing term in Eq. (15b) is proportional to a^2 . The amplitudes attenuate landward, and the attenuation speed increases with the wave number a .

Fig. 3 demonstrates the following information. The pure tidal loading effect leads to negative phase shifts, i.e., time-advance, in aquifer near the shore. The smaller the wave number, the smaller the negative phase shift. The phase shift increases landward, and the increasing speed becomes larger as the wave number a increases. On the coastline, the smallest negative phase shift is about -0.7 (Fig. 3c, $x = 0$), which corresponds to a time-advance of about 2.7 h for diurnal tide (1.35 h for semidiurnal tide). Negative phase shift near shoreline has been observed in reality (e.g., Maas and De Lange, 1987). Since the phase shift is negative and increases landward, there will be one inland place where the phase shift is zero (e.g., at $x = 14 \text{ m}$ in Fig. 3a). In this case the groundwater head will fluctuate synchronously with the tide. This was also observed in reality (e.g., Cheng et al., 2004). Maas and De Lange (1987) and Li et al. (2007) also showed that the observed negative or zero phase shifts were due to the dominant tidal loading effect.

Figs. 4–6 reported the spatial variations of the head fluctuation amplitude induced by the pure leakage effect given by $|W_{\text{leakage}}|$ in aquifer near the shore for different values

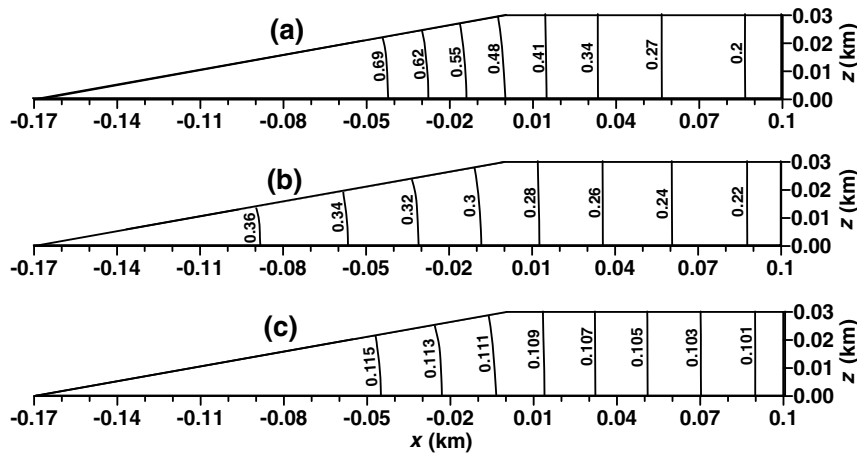


Figure 2 The spatial variation of the head fluctuation amplitude $|W_{\text{loading}}|$ induced by the pure, unit tidal loading effect ($L_e = 1$, $\sigma = 0$) in aquifer near the shore when the wave number a equals (a) 0.01 m^{-1} , (b) 0.0032 m^{-1} and (c) 0.001 m^{-1} . The slope $\theta = 10^\circ$.

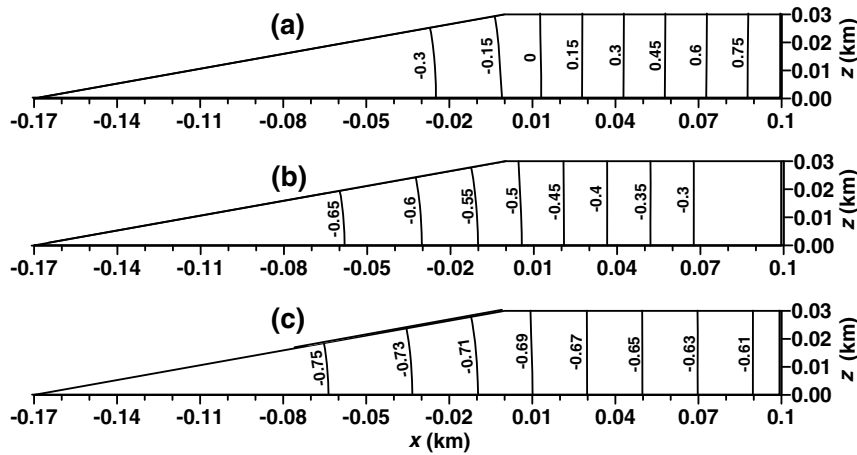


Figure 3 The spatial variation of the phase shift $\arg(W_{\text{loading}})$ induced by the pure, unit tidal loading effect ($L_e = 1$, $\sigma = 0$) in aquifer near the shore when the wave number a equals (a) 0.01 m^{-1} , (b) 0.0032 m^{-1} and (c) 0.001 m^{-1} . The slope $\theta = 10^\circ$.

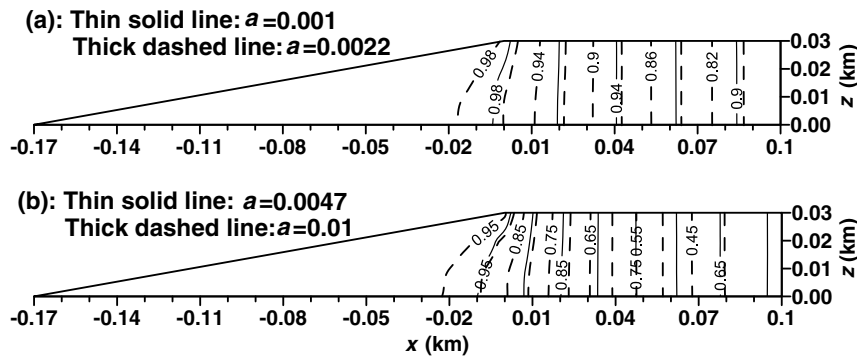


Figure 4 The spatial variations of the head fluctuation amplitude $|W_{\text{leakage}}|$ induced by the pure leakage effect ($\sigma = 100.0$, $L_e = 0$) in aquifer near the shore when the wave number a equals (a) 0.001 m^{-1} and 0.0022 m^{-1} ; (b) 0.0047 m^{-1} and 0.01 m^{-1} . The slope $\theta = 10^\circ$.

of the dimensionless leakage σ and the wave number a . The following can be observed from Figs. 4–6. The head fluctuation amplitude near the offshore aquifer increases

with the dimensionless leakage σ and decreases with the wave number a . When σ is very large, the outlet-capping approaches Dirichlet boundary condition and the tidal head

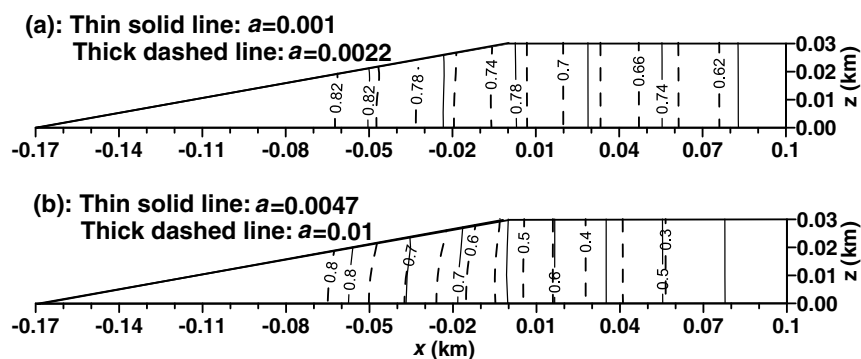


Figure 5 The spatial variations of the head fluctuation amplitude $|W_{\text{leakage}}|$ induced by the pure leakage effect ($\sigma = 1.0$, $L_e = 0$) in aquifer near the shore when the wave number a equals (a) 0.001 m^{-1} and 0.0022 m^{-1} ; (b) 0.0047 m^{-1} and 0.01 m^{-1} . The slope $\theta = 10^\circ$.

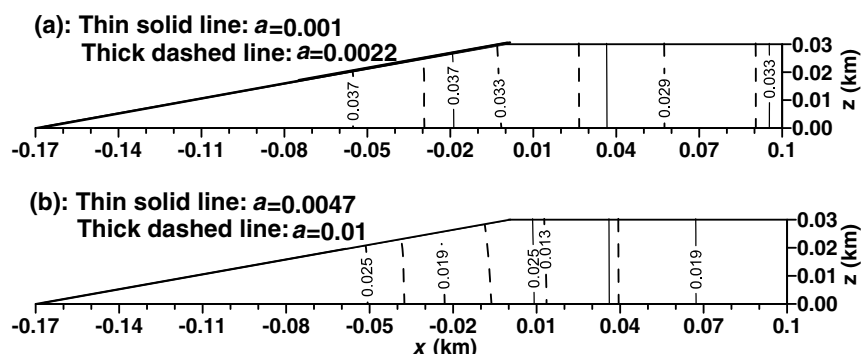


Figure 6 The spatial variations of the head fluctuation amplitude $|W_{\text{leakage}}|$ induced by the pure leakage effect ($\sigma = 0.01$, $L_e = 0$) in aquifer near the shore when the wave number a equals (a) 0.001 m^{-1} and 0.0022 m^{-1} ; (b) 0.0047 m^{-1} and 0.01 m^{-1} . The slope $\theta = 10^\circ$.

fluctuation amplitude at the outlet-capping due to the pure leakage effect approaches 1.0 (see Fig. 4). The amplitude attenuates landward and the attenuating speed increases with the wave number a . When σ is very small, the outlet-capping approaches a no-flow boundary condition and the tidal head fluctuation amplitude due to the pure leakage effect tends to vanish (see Fig. 6).

Figs. 7–9 reported the spatial variations of the phase shift $\arg(W_{\text{leakage}})$. The following observations can be made

from Figs. 7–9. The pure leakage effect always leads to positive phase shifts in aquifer near the shore. The phase shift in the offshore aquifer increases with the wave number a and decreases with the dimensionless leakance σ . When a is sufficiently small and σ is sufficiently large, the phase shift at the coastline approaches zero (see Fig. 7a). On the contrary, when a is sufficiently large and σ is sufficiently small, the phase shift at the coastline may be as large as 1.6 (see Fig. 9b), corresponding to a very long time lag of 6.3 h

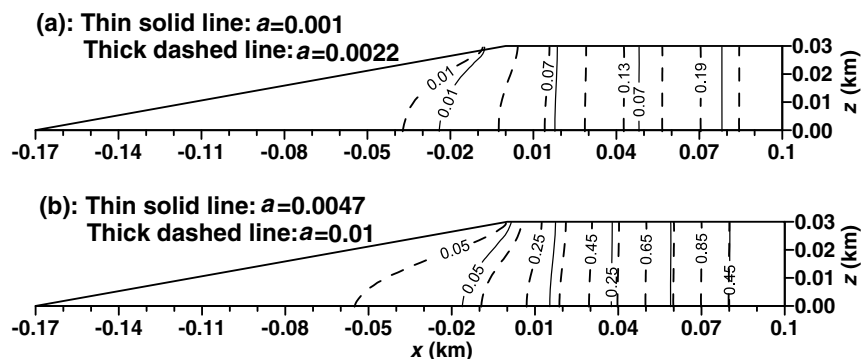


Figure 7 The spatial variations of the phase shift $\arg(W_{\text{leakage}})$ induced by the pure leakage effect ($\sigma = 100.0$, $L_e = 0$) in aquifer near the shore when the wave number a equals (a) 0.001 m^{-1} and 0.0022 m^{-1} ; (b) 0.0047 m^{-1} and 0.01 m^{-1} . The slope $\theta = 10^\circ$.

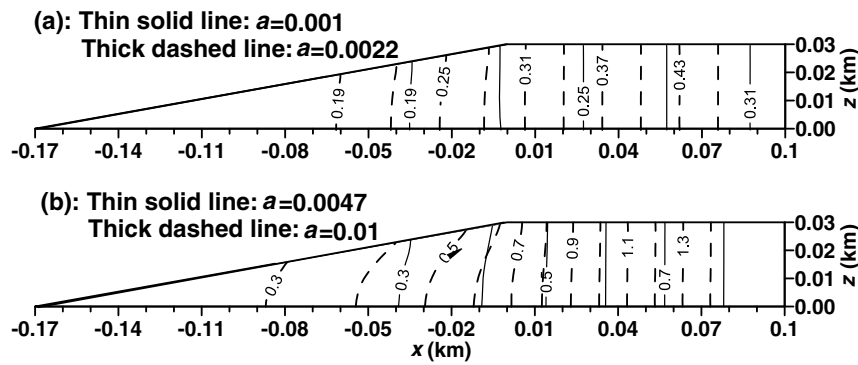


Figure 8 The spatial variations of the phase shift $\arg(W_{\text{leakage}})$ induced by the pure leakage effect ($\sigma = 1.0$, $L_e = 0$) in aquifer near the shore when the wave number a equals (a) 0.001 m^{-1} and 0.0022 m^{-1} ; (b) 0.0047 m^{-1} and 0.01 m^{-1} . The slope $\theta = 10^\circ$.

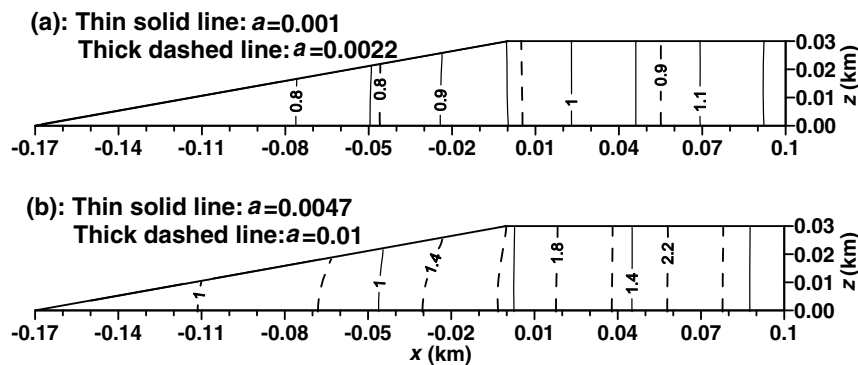


Figure 9 The spatial variations of the phase shift $\arg(W_{\text{leakage}})$ induced by the pure leakage effect ($\sigma = 0.01$, $L_e = 0$) in aquifer near the shore when the wave number a equals (a) 0.001 m^{-1} and 0.0022 m^{-1} ; (b) 0.0047 m^{-1} and 0.01 m^{-1} . The slope $\theta = 10^\circ$.

for diurnal tide (3.15 h for semidiurnal tide). The phase shift increases with the landward distance, and the increasing speed becomes larger as the wave number a increases.

In Figs. 2–9, the contour lines in the offshore part of the aquifer are not vertical, indicating that significant 2-dimensional flow occurs there. In Figs. 2 and 3, due to the no-flow boundary conditions at the outlet-capping and the aquifer bottom, the contour lines in the offshore aquifer are perpendicular to the boundary and bulge in the up-right direction, which implies that both the relative amplitude and the absolute value of the phase shift increase with depth. In Figs. 4, 5, 7 and 8 ($\sigma \geq 1$), the boundary condition at the outlet-capping is dominated by the leakage, the contour lines in the offshore aquifer bulge in the up-left direction, which implies that both the relative amplitude and the absolute value of the phase shift decrease with depth. The contour lines gradually become vertical and the tidal flow becomes essentially horizontal as the landward distance from the coastline increases.

Analyses of the joint effects of the leakage and loading forcing terms

In this section, the joint effects of the leakage through the outlet-capping and the tidal loading will be discussed. In the ideal case of $\theta = 90^\circ$, the analytical solution (1a) applies. In

this case, there is neither vertical flow nor tidal loading effect, and the relative head fluctuation amplitude along the coastline $x = 0$ is simply given by $\sigma / \sqrt{\sigma^2 + 2\sigma + 2}$, and the phase shift at $x = 0$ is $\arctan [1 / (1 + \sigma)]$. Given the tidal head fluctuations at the coastline, the inland head fluctuations can be easily determined using the simple 1-dimensional solution of Jacob (1950) because flow in the inland aquifer is approximately horizontal, as is shown in previous section. Due to this reason, our analyses in this section will focus on the location $x = 0 \text{ m}$, $z = 15 \text{ m}$ at the coastline (see Fig. 1).

Fig. 10 shows how the head fluctuation amplitude (left panel) and the phase shift (right panel) at the location M ($x = 0 \text{ m}$, $z = 15 \text{ m}$) change with the wave number a for different values of the slope θ , the dimensionless leakance σ and the tidal loading efficiency L_e . The following observations can be made from the left panel of Fig. 10.

For aquifer with large outlet-capping leakance ($\sigma \geq O(1)$), the 3 left plots of Fig. 10a–c), the high leakance through the outlet-capping overwhelms the tidal loading effect. In this case, the relative amplitude becomes insensitive of the change of L_e . In particular, when $\sigma = 100$, the results (not shown) for $L_e = 0.5$ are almost the same as those for $L_e = 0.9$. The relative amplitude at M decreases with the wave number a because greater value of a corresponds to smaller aquifer diffusivity which causes stronger attenuation of the tidal waves when they propagate from the outlet

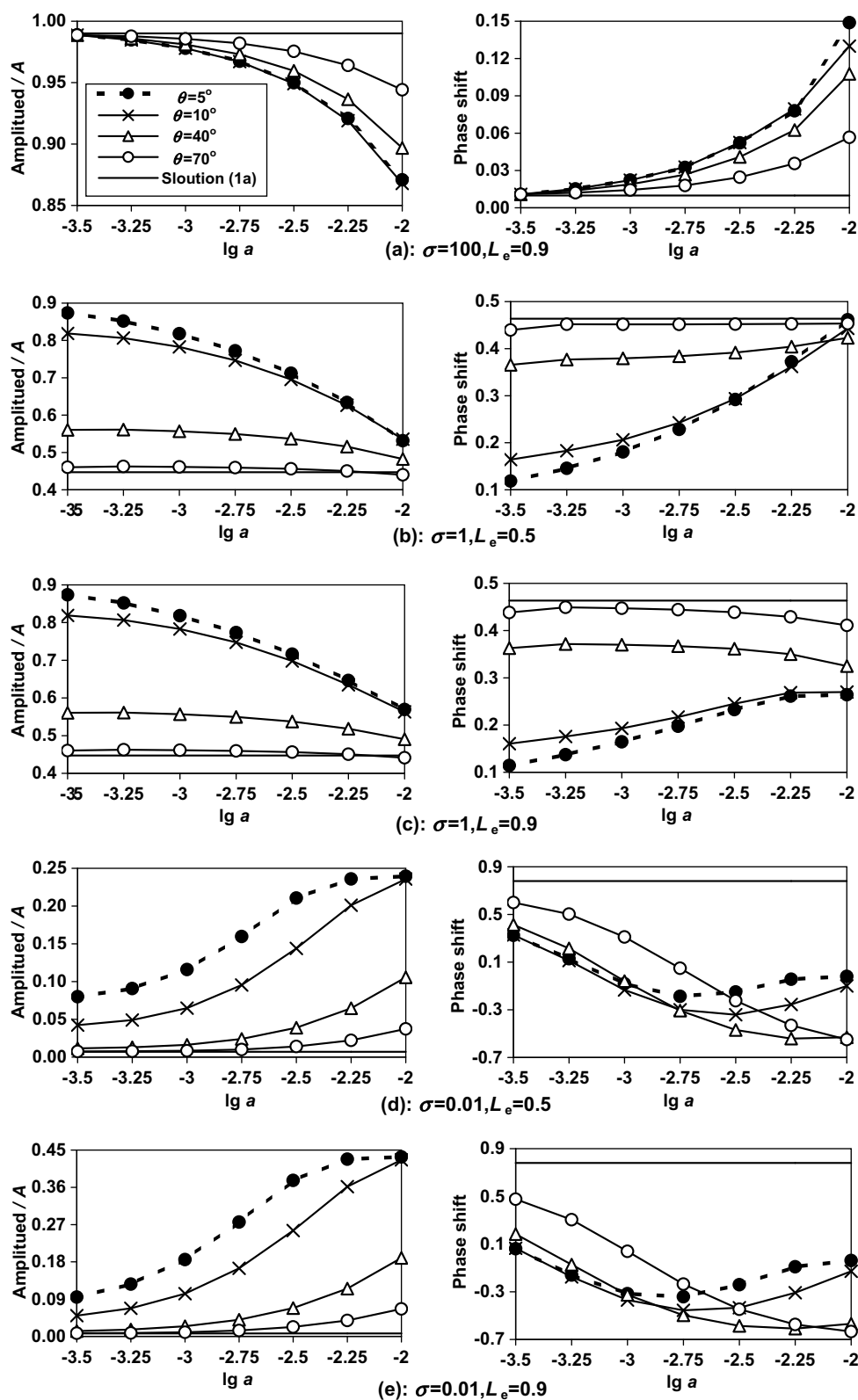


Figure 10 Changes of relative head fluctuation amplitude (left panel) and phase shift (right panel) at the location M ($x = 0$ m, $z = 15$ m) with the wave number a for different values of slope θ when the dimensionless leakage σ and the tidal loading efficiency L_e equal (a) $\sigma = 100, L_e = 0.9$, (b) $\sigma = 1, L_e = 0.5$, (c) $\sigma = 1, L_e = 0.9$, (d) $\sigma = 0.01, L_e = 0.5$, and (e) $\sigma = 0.01, L_e = 0.9$. (The case for $\sigma = 100, L_e = 0.5$ is almost the same as the case (a) and not shown here.)

to the point M. The relative amplitude increases with the slope θ for aquifers with larger leakage ($\sigma = 100$) because

the distance between the outlet boundary and the point M is shorter for larger slope.

For aquifer with small outlet-capping leakance ($\sigma = 0.01$, the 2 left plots of Fig. 10d and e), the tidal loading effect dominates and the hydraulic impact through the outlet-capping becomes negligible. In this case, the relative amplitude at M becomes sensitive to L_e . It increases with L_e and the wave number a . This is because the dominant driven forcing is the tidal loading specified by the term $a^2 L_e$ in the governing Eq. (15b). In Fig. 10d and e, the amplitude also increases when the slope θ decreases, which becomes particularly distinct for larger values of L_e and a . Physically, the tidal loading effect strongly depends on the aquifer's offshore extent $b \cot\theta$. The greater the value of $b \cot\theta$, the stronger the tidal loading effect will be. Because smaller slope θ corresponds to longer offshore extent of the aquifer, it leads to stronger tidal head fluctuations.

Comparison of the curves with the same values of a , θ and L_e in the five plots in left panel of Fig. 10 indicated that the relative amplitude always increases with the dimensionless leakance σ of the outlet-capping.

The following observations can be made from the right panel of Fig. 10. For aquifers with dominant outlet-capping leakance ($\sigma = 100$, right plot of Fig. 10a), the phase shift is always positive and increases with the wave number a for any slopes. For aquifers with dominant tidal loading ($\sigma = 0.01$, right plots of Fig. 10d and e), negative phase shifts occur. In general (right plots of Fig. 10b–e), however, the phase shift of the numerical solutions is not monotonic with respect to the slope θ , the tidal loading efficiency L_e , and the wave number a . This is due to the superposition of the tidal loading effect and the leakage through the outlet-capping.

The analytical solution (1a) neglected the vertical flow and assumed a vertical outlet-capping at the coastline, which implies a zero offshore extent and no tidal loading effect. Therefore, the analytical and numerical solutions agree well with each other only when both the vertical flow and the tidal loading effect onto the offshore extending portion are insignificant. This can be seen from the comparisons of the numerical solutions with the analytical solution (1a) in Fig. 10, where they are close to each other when both of the following two conditions hold: (i) the slope of the outlet-capping is big and/or the leakance of the outlet-capping is great and overwhelms the tidal loading effect, (ii) the aquifer has a sufficiently great hydraulic diffusivity (small value of a) so that the damping effect on the tidal wave propagation in the vertical direction can be neglected.

Conclusions

The submarine outlet of a coastal confined aquifer is usually covered by a sloping outlet-capping such as silt and fine sands. This paper focuses on the impacts of the slope of the outlet-capping on the tide-induced head fluctuations in the coastal confined aquifer. The time-dependent mathematical model for a typical coastal aquifer configuration was first transformed into a time-independent model using Fourier transform method introduced by Li et al. (2006). With a typical aquifer thickness of 30 m, the model has four independent parameters: tidal wave propagation parameter a , the dimensionless leakance σ and the slope θ of the outlet-capping and the tidal loading efficiency L_e . A series of

numerical simulation was conducted for various typical values of the four model parameters to investigate the effects of the tidal loading, the leakance of the outlet-capping when the slope θ varies from 5° to 90° . The numerical solution was first verified by the Li et al. (2007) analytical solution when $\theta = 90^\circ$.

The analyses of the numerical solutions demonstrated that the effect of the slope of the outlet-capping on the tide-induced head fluctuations in the aquifer is usually significant. The combined actions of the tidal loading, the slope, the aquifer diffusivity and the leakage of the outlet-capping lead to complicated head fluctuation behavior and 2-dimensional flow in the aquifer near the shore. For aquifers with great hydraulic diffusivity, large slope and/or large outlet-capping leakance, the tidal loading effect is relatively weak and the leakance through the outlet-capping dominates. In this case the analytical solution applies. For aquifers with small hydraulic diffusivity, small slope and/or small outlet-capping leakance, the outlet acts approximately as a no-flow boundary condition and the tidal loading dominates. In this case negative or very small phase shifts occur near the coastline.

In reality, the hydrogeological information is much more difficult to obtain in submarine aquifers than in inland aquifers. The theoretical and numerical investigations of this paper may provide some guides and methods to infer the submarine aquifer structures and parameters from inland observations. For example, if the observed tidal head fluctuation near the coastline has a negative phase shift with respect to the tidal level fluctuation, one may tend to conclude that the offshore aquifer is dominated by tidal loading effect and there is no direct hydraulic connection between the aquifer and the seawater near the shore.

Acknowledgment

This research was supported by the National Natural Science Foundation of China (No. 40672167) and the 111 Project (B08030). We are grateful to the 2 anonymous reviewers for their helpful comments which lead to significant improvement of the manuscript.

References

- Carr, P.A., 1971. Use of harmonic analysis to study tidal fluctuations in aquifers near the sea. *Water Resour. Res.* 7 (3), 632–643.
- Carr, P.A., van der Kamp, G., 1969. Determining aquifer characteristics by the tidal methods. *Water Resour. Res.* 5 (5), 1023–1031.
- Cartwright, N., Nielsen, P., Li, L., 2004. Experimental observations of watertable waves in an unconfined aquifer with a sloping boundary. *Adv. Water Resour.* 27 (10), 991–1004.
- Cheng, J.M., Chen, C.X., Ji, M.R., 2004. Determination of aquifer roof extending under the sea from variable-density flow modelling of groundwater response to tidal loading: case study of the Jahe River Basin, Shandong Province, China. *Hydrogeol. J.* 12 (4), 408–423.
- Erskine, A.D., 1991. The effect of tidal fluctuation on a coastal aquifer in the U.K. *Ground Water* 29 (4), 556–562.
- Ferris, J.G., 1951. Cyclic fluctuations of water level as a basis for determining aquifer transmissibility. *Int. Assoc. Sci. Hydrol. Publ.* 33, 148–155.

- Gregg, D.O., 1966. An analysis of ground-water fluctuations caused by ocean tides in Glynn County, Georgia. *Ground Water* 4 (3), 24–32.
- Guo, Q.N., Li, H.L., Boufadel, M.C., Xia, Y.Q., Li, G.H., 2007. Tide-induced groundwater head fluctuation in coastal multi-layered aquifer systems with a submarine outlet-capping. *Adv. Water Resour.* 30, 1746–1755, doi:10.1016/j.advwatres.2007.01.003.
- Jacob, C.E., 1940. On the flow of water in an elastic artesian aquifer: American Geophysical Union Transactions, part 2, pp. 547–586; duplicated 1953 as US Geological Survey Ground Water Note 8.
- Jacob, C.E., 1950. Flow of groundwater. In: Rouse, H. (Ed.), *Engineering Hydraulics*. John Wiley, New York, pp. 321–386.
- Jeng, D.-S., Li, L., Barry, D.A., 2002. Analytical solution for tidal propagation in a coupled semi-confined/phreatic coastal aquifer. *Adv. Water Resour.* 25 (5), 577–584.
- Jiao, J.J., Tang, Z., 1999. An analytical solution of groundwater response to tidal fluctuation in a leaky confined aquifer. *Water Resour. Res.* 35 (3), 747–751.
- Li, G., Chen, C., 1991a. Determining the length of confined aquifer roof extending under the sea by the tidal method. *J. Hydrol.* 123, 97–104.
- Li, G., Chen, C., 1991b. The determination of the boundary of confined aquifer extending under the sea by analysis of groundwater level fluctuations. *Earth Sci.* 16, 581–589 (in Chinese).
- Li, H.L., Jiao, J.J., 2001a. Tide-induced groundwater fluctuation in a coastal leaky confined aquifer system extending under the sea. *Water Resour. Res.* 37 (5), 1165–1171.
- Li, H.L., Jiao, J.J., 2001b. Analytical studies of groundwater-head fluctuation in a coastal confined aquifer overlain by a leaky layer with storage. *Adv. Water Resour.* 24 (5), 565–573.
- Li, H.L., Jiao, J.J., Luk, M., Cheung, K., 2002. Tide-induced groundwater level fluctuation in coastal aquifers bounded by L-shaped coastlines. *Water Resour. Res.* 38 (3), 6-1–6-8.
- Li, H.L., Jiao, J.J., Tang, Z.H., 2006. Semi-numerical simulation of groundwater flow induced by periodic forcing with a case-study at an island aquifer. *J. Hydrol.* 327, 438–446.
- Li, H.L., Li, G.Y., Cheng, J.M., Boufadel, M.C., 2007. Tide-induced head fluctuations in a confined aquifer with sediment covering its outlet at the sea floor. *Water Resour. Res.* 43. doi:10.1029/2005WR00472.
- Li, L., Barry, B.A., Stagnitti, F., Parlange, J.-Y., 1999. Submarine groundwater discharge and associated chemical input to a coastal sea. *Water Resour. Res.* 35, 3253–3259.
- Li, L., Barry, D.A., Cunningham, C., Stagnitti, F., Parlange, J.-Y., 2000a. A two-dimensional analytical solution of groundwater response to tidal loading in an estuary and ocean. *Adv. Water Resour.* 23 (8), 825–833.
- Li, L., Barry, D.A., Stagnitti, F., Parlange, J.-Y., Jeng, D.-S., 2000b. Beach water table fluctuations due to spring-neap tides: moving boundary effects. *Water Resour.* 23, 817–824.
- Maas, C., De Lange, W.J., 1987. On the negative phase shift of groundwater tides near shallow tidal rivers – The Gouderak anomaly. *J. Hydrol.* 92, 333–349.
- Merritt, M.L., 2004. Estimating Hydraulic Properties of the Floridan Aquifer System by Analysis of Earth-Tide, Ocean-Tide, and Barometric Effects, Collier and Henry Counties, Florida. USGS/Water-Resources Investigations Report, 4203–4267.
- Nielsen, P., 1990. Tidal dynamics of the water table in beaches. *Water Resour. Res.* 26 (9), 2127–2134.
- Pinder, G.F., Gray, W.G., 1977. *Finite Element Simulation in Surface and Subsurface Hydrology*. Academic Press, New York.
- Sun, H., 1997. A two-dimensional analytical solution of groundwater response to tidal loading in an estuary. *Water Resour. Res.* 33 (6), 1429–1435.
- Townley, L.R., 1995. The response of aquifers to periodic forcing. *Adv. Water Resour.* 18 (3), 125–146.
- van der Kamp, G., 1972. Tidal fluctuations in a confined aquifer extending under the sea. *Int. Geol. Cong.* 24, 101–106.
- Xia, Y.Q., Li, H.L., Boufadel, M.C., Guo, Q.N., Li, G.H., 2007. Tidal wave propagation in a coastal aquifer: effects of leakages through its submarine outlet-capping and offshore roof. *J. Hydrol.* 337, 249–257. doi:10.1016/j.jhydrol.2007.01.036.